ERRATUM

DESY 80/83
September 1980

CENTRAL DETECTORS / by A. Wagner

pg 3, line 5 of last paragraph : .., N the number of ... should be
..., (N+1) the number of

pg 3, line 6 of last paragraph : $A'_N = 750$ should be $A'_N = 720$

pg 4, formula 3 : 0.15 should be 0.015.

DEUTSCHES ELEKTRONEN-SYNCHROTRON DESY

DESY 80/83
September 1980

CENTRAL DETECTORS

by

A. Wagner
Physikalisches Institut der Universität Heidelberg

NOTKESTRASSE 85 · 2 HAMBURG 52

To be sure that your preprints are promptly included in the
HIGH ENERGY PHYSICS INDEX ,
send them to the following address (if possible by air mail) :

DESY
Bibliothek
Notkestrasse 85
2 Hamburg 52
Germany

DESY 80/83
September 1980

Central Detectors

A. Wagner

Physikalisches Institut der Universität Heidelberg

Invited paper presented at the International Conference on Experimentation at LEP,
Uppsala, 16 - 20 June 1980.

1. INTRODUCTION

In March 1976 a discussion meeting on PETRA experiments took place in Frascati. At that time cylindrical track detectors were in their infancy. MARK I, with a spark chamber at the SPEAR storage ring, PLUTO, with a multiwire proportional chamber [1], and the DESY-Heidelberg detector [2] with a 6-layer cylindrical driftchamber, both at the DORIS storage ring, were all taking data. The driftchambers of the CCOR detector [3] at CERN were under construction and the first tests were being made on the large driftchamber system of the MARK II detector [4].

Around the same time ideas for the next generation of central detectors were already under discussion [5,6]. These detectors became known as pictorial- or imaging driftchambers since the aim was to record a complete picture of particle trajectories even in the case of complex events.

At the time of the 1980 Uppsala meeting on Experimentation at LEP only one of the detectors mentioned so far has ceased to exist (MARK I) while most others are taking data. The great success of cylindrical driftchambers due to their reliability, accuracy and moderate number of readout channels has led meanwhile to their application in a large number of new detectors at CESR, DCI, DORIS, ISR, PEP, PETRA, and SPEAR.

Based on the experience of the last years it is a commonly held belief that cylindrical driftchambers, combined in most cases with a solenoidal magnet, are the optimal solution to the problem of track detection, momentum measurement and possibly even particle identification in e^+e^- storage ring experiments.

The physics of the driftprocess and its inherent limitations are summarized elsewhere [7]. It is the aim of this report to give first (in chapter 2) a review of the main types of central detectors presently under operation or construction. It is not intended to be a detailed summary of all parameters of all detectors but rather to provide a critical comparison of the different methods of measurement.

The main emphasis is put on the question : What limits the chamber resolution? In chapter 3 the space resolution in the Rφ-plane is discussed. The different methods to determine the coordinate along the cylinder axis (z) and the corresponding resolutions are presented in chapter 4. The drift-chamber electronics is discussed in chapter 5 with emphasis on the electronics of pictorial driftchambers. An important aspect of any track chamber is its double track resolution (chapter 6). Chapters 7 and 8 contain comments on particle identification through measurement of dE/dx in the driftchamber and on calibration. The report concludes with an extrapolation of the present experience, especially that gained with pictorial driftchambers, to LEP and with the discussion of some open questions.

The goal in the construction of central detectors is the measurement of momenta, directions and multiplicity of charged particles with the highest possible accuracy, even in regions of high local track density as for example in e^+e^- annihilations at high energies.

The momentum resolution of the detector has two contributions [8]. The first one is due to measurement errors on the coordinates of the track points :

$$\left(\frac{\delta p_T}{p_T}\right)_m = \frac{p_T}{0.03} \frac{\sigma_{R\phi}}{L^2 B} \sqrt{\frac{A'_N}{(N+5)}} \qquad (1)$$

Here p_T is the transverse momentum, $\sigma_{R\phi}$ the measurement error in the Rφ-plane, L the radial track length, B the magnetic field, N the number of equally spaced points on the track and A'_N a statistics factor, $A'_N = 750$. The units are GeV/c, kG, m. The easiest way therefore to improve $\Delta p_T/p_T$ is to increase L. But the detector volume and price grow like L^3, so this solution is rather expensive. Other ways of improving the resolution require a larger magnetic field or a smaller $\sigma_{R\phi}$. The resolution improves further with the number of measured points on the track, but only like $1/\sqrt{N}$.

The second contribution to the momentum resolution is due to multiple scattering :

$$\left(\frac{\delta p_T}{p_T}\right)_{ms} = 0.5 \frac{1}{LB} \sqrt{\frac{L}{X_o} \cdot C_N} \qquad (2)$$

Here L/X_o is the amount of material in the chamber in units of a radiation length, and C_N is another statistical factor, $C_N = 1.43$. This contribution does not depend on momentum and dominates the resolution at low momenta. The momentum p_X for which both contributions are equal can be obtained from formulae (1) and (2) :

$$p_X = 0.15 \frac{L}{\sigma_{R\phi}} \sqrt{\frac{L}{X_o} \frac{C_N}{A'_N} (N+5)} \qquad (3)$$

p_X is proportional to L and $1/\sigma_{R\phi}$.

The error on the total momentum of the track

$$p = p_T / \sin\theta \qquad (4)$$

contains in addition a contribution from the longitudinal coordinate uncertainty, σ_z, which determines the error on the polar angle θ :

$$(\delta\theta)_m = \frac{\sigma_z}{L} \sqrt{\frac{12\ N}{(N+1)(N+2)}} \qquad (5)$$

Here again the multiple Coulomb scattering adds a second term

$$(\delta\theta)_{ms} = \frac{.015}{\sqrt{3}} \frac{1}{p\beta} \sqrt{\frac{L}{X_o}} \qquad (6)$$

2. TWO GENERATIONS OF DRIFTCHAMBERS

2.1 Classical driftchambers

The type of driftchamber which is called "classical" in this context has approximately the following characteristics : The chamber contains typically 15 - 20 layers of wires (points per track). For approximately half of these layers the wires are oriented parallel to the beam and magnetic field axis. The other wire planes are rotated by a small stereo angle (typically $\pm 3^{o}$) with respect to this axis. The zero degree planes are used for pattern recognition, the stereo planes provide the z-coordinate of the reconstructed tracks. The individual driftcells have a simple structure of a sense wire and a triplet of potential wires (Fig. 1). This pattern is repeated around the circumference. Radially the cells are in most cases open. The longest drift distances are typically 1 - 2 cm.

The appealing feature of this construction is its simplicity and minimal number of potential wires. On the other hand field shaping to compensate for the influence of the magnetic field is not possible. Therefore the simple time to space relation of an ideal driftchamber with linear drift trajectories

$$d = V_D \cdot t \qquad (7)$$

where d is the drift distance, t the measured drift time and V_D the drift velocity, can no longer be applied.

The first cylindrical driftchamber of this type was the central detector of the MARK II experiment [4]. A number of other detectors have followed, two of which will be described here as examples. The first is the TASSO detector [9] at the DESY storage ring PETRA. Fig. 1a shows a cross section through the drift chamber, Fig. 1b illustrates the details of the cell structure. This chamber has 15 layers, 9 of which have their wires parallel to the beam axis, with a total of 2340 sense wires. The radial track length L is 85.5 cm. Not shown in Fig. 1a is a set of four cylindrical proportional wire chambers sitting between the beam pipe and the driftchamber. The solenoid provides a uniform magnetic field of 5 KG. Fig. 2 shows the Rϕ-view of an event of the type

$e^+e^- \rightarrow$ hadrons at an energy of E_{cm} = 30 GeV. In this picture the information of the 0^{o} planes and the proportional wire chambers is displayed.

As a second example the chamber system of the CELLO detector [10] is discussed. It differs in two respects from the TASSO chamber. First, the chamber is smaller in diameter (radial track length L = 55 cm) but operates in a magnetic field of 13 KG, and second, the chamber contains 12 equally spaced layers of chambers (Fig. 3), 5 of which are proportional chambers with cathode read out. These chambers provide the z-coordinates of the tracks and the main information for the track trigger in the Rϕ- and Rz-plane. The 7 other layers are driftchambers all of which have their wires at 0^{o}. The basic structure of the driftcell is the same as that of the TASSO chamber. Fig. 4 shows a multihadron event as seen by the CELLO chamber.

The addition of two more potential wires per cell, one above and one below the anode wire improves the homogenuity of the electric field. This technique is applied for example in the DM2 [11] magnetic detector at the DCI-storage ring.

2.2 Pictorial driftchambers

In this type of chamber a large number of points (40 - 200) is recorded for each track. In contrast to the classical driftchambers true space points are measured. The high density of space points helps to analyse events with a large number of tracks concentrated in a small region of the chamber (jets), and to find secondary vertices and decays in the chamber volume. The multiple sampling along each track makes particle identification possible through the measurement of the energy loss in the chamber gas.

The high granularity in the radial direction is combined with a high granularity in the azimuthal direction in order to resolve tracks close to each other. This can be best achieved by using multihit electronics combined with large drift cells, with drift distances typically from 3 to 18 cm. (the TPC solution is different and will be discussed below). Because of the large driftcells a great fraction of all drift trajectories are linear and relation (7) is true, leading to a simple time-to-space relation.

On the other hand one has to be careful that the electron diffusion does not spoil the resolution due to the long average drift path.

There are at present two pictorial driftchambers in operation, in the experiment JADE [6] at PETRA and the AFS [12] at the CERN ISR. Both will be discussed as examples. As a third case the central detector of the UA1 [13] experiment at the $\bar{p}p$ collider at CERN will be described. This detector is under construction. In all these chambers the electric and magnetic fields are orthogonal to each other.

The idea for the "jet chamber" of the JADE detector was first presented in 1976 at the Frascati Meeting on PETRA experiments. Fig. 5 shows a cross section through 2 out of 24 independent segments (each 15^0 wide) which form the full cylindrical chamber. Each segment contains 4 cells with 16 anode wires, separated by potential wires. The total number of sense wires is 1536. The equipotential planes of the drift field are parallel to the wire plane. Kapton foils carrying parts of the field shaping electrodes provide the boundaries between neighbouring cells. Since the chamber is operated in a magnetic field of 4.5 KG orthogonal to the drift field the drift trajectories are tilted by 18.5^0.

Up to 48 space points are measured along each track. The radial track length is 57 cm, the longest drift path 7.5 cm. The wire position and drift time determine the R and ϕ coordinates. The longitudinal coordinate z, measured along the wire, (L_W = 234 cm), is given by the charge division method. The chamber is operated with a gas mixture of argon, methane and isobutane at a pressure of 4 atm. The operation under pressure helps to improve the space resolution by reducing electron diffusion and allows for better particle identification by measurement of the energy loss. Fig. 6 shows a typical jet event with a charged multiplicity of 12. Each track can be clearly recognized even without track fitting, illustrating the meaning of the name "pictorial driftchamber".

The central detector of the axial field spectrometer (AFS), shown in Fig. 7, is in principal very similar to the "jet chambers" of JADE. There are some differences however in the construction : The chamber is built from two independent half cylinders. The azimuthal segmentation is 4 degrees,

giving a maximum drift path of 2.8 cm. The cell boundaries are made from wires, not from foils. This leads to cross talk between neighbouring segments for tracks closer than 4 mm to the boundary. Up to 42 space points are measured along each track. The total number of sense wires is 3400. Charge division is used to determine the z coordinate (wire length L_W = 128 cm). The chamber is operated with Ar/C_2H_6 at atmospheric pressure. The energy loss of the particles in the gas is measured. Fig. 8 shows a typical event in the AFS.

The central detector of the UA1 experiment at the CERN $\bar{p}p$ collider, which is presently under construction, differs considerably from the chambers of JADE and AFS. Since the expected particle distribution requires good momentum resolution also in very forward direction a dipol magnet was chosen. The track detector is made from 6 half-shells, two for the central chamber and four for the forward chambers (Fig. 9).

The principle of the chamber can be best understood by looking at Fig. 9b. Particles emerging in forward direction from the interaction region move parallel to the anode planes. The electrons drift over a maximum distance of 18 cm to the anode wires in an electric field which is orthogonal to the magnetic field. The chamber modules are about 1.9 m long and give on the order of 180 points on each track. In the central chamber which is used to measure tracks emerging under large polar angles the wire planes are put orthogonal to the beam. Here up to 100 points are measured on a track. The third coordinate is obtained by charge division on the 6100 sense wires.

The most radical concept of a pictorial driftchamber is that of the time projection chamber [5] (TPC). Fig. 10 gives a schematical representation of the chamber. The whole chamber volume is free of material except for the counting gas. A central high voltage electrode provides a drift field in direction of both end plates. The electrons therefore drift over a very large distance of up to 1 meter. Since the chamber sits in a solenoid magnet (15 KG), magnetic field and drift field are parallel. The entire chamber read-out is concentrated at the end plates, each of which is subdivided into six sectors. Each sector contains 186 sense wires to measure the arrival time of the drifting electrons (z-coordinate) and to sample the energy loss of the particles in the gas. Underneath 15 of the

anode wires sit rows of inductive pads (8 x 8 mm^2), equally spaced in R. The induced signal on these pads provides the Rϕ coordinate. Further details and plans for future development are described elsewhere [14].

The TPC is designed to work at a pressure of 10 atm. in order to obtain good particle identification. The concept of the TPC is elegant, the technical realization of the chamber however is difficult, mainly due to the very high voltages involved and the large number of read out channels (14.000).

In Fig. 11 a summary of chamber dimensions, radial track length and maximal drift length, is shown for all the detectors discussed in this chapter.

2.3 Left-right ambiguity

From the measurement of the timing on one sense wire only the distance of a track from the wire can be derived, but not the side at which it passed the wire. This ambiguity is resolved in different ways : In the small drift cell configuration each drift time is transformed into 2 coordinates ($\pm$ d). The subsequent pattern recognition decides which sign is correct. In a chamber configuration like JADE (Fig. 5) a track normally stays on one side of a wire plane. In order to resolve in this case the left-right ambiguity the anode wires are displaced by a small amount δ with respect to the plane of potential wires, alternatingly to one side and the other. The amount of staggering is $\pm$ 150 µm for JADE, $\pm$ 400 µm for AFS. This staggering is further enlarged through electrostatic deflection. This arrangement provides a unique resolution of the ambiguity [15].

In the case of the UA1 detector the left-right ambiguity is resolved by replacing one plane of anode wires by two planes, for left and right tracks, as shown in the insert of Fig. 9b.

3. SPACE RESOLUTION IN THE Rϕ PLANE

The Rϕ coordinates are determined except in the case of the TPC, from the wire positions and the measured drift times. In order to understand the observed chamber resolutions the possible sources of errors are discussed : wire positioning, time measurement and time-to-space relation.

3.1 Wire position inaccuracy

The position inaccuracy has a random and a systematic contribution. The random contribution is given by the wire support. There are two construction techniques to support wires in cylindrical driftchambers. In the most common one holes are drilled with high precision into large endplates which carry all wires. Into these holes insulating feed-throughs are introduced which support and position the wires. The accuracy of this method as quoted by different experiments is : MARK II 100 µm, TASSO 120 µm, AFS 20 µm. A second method is used in the JADE chamber : all 16 wires of one cell are held by a comb-like structure manufactured with high precision. This guarantees a good relative accuracy within one cell (10 - 20 µm).

There are several sources for systematic uncertainties in the knowledge of the wire position. Corrections for these effects can only be roughly calculated. Gravitational sagging and electrostatic deflection (for JADE 70 µm and 50 µm, respectively) vary as function of the z coordinate and have their maximum value in the center of the detector. Care has to be taken to align the two endplates with respect to each other since a rotation would introduce an apparent momentum.

3.2 Time measurement

Errors in the timing measurement occur through timing fluctuations, imperfect timing corrections and the finite resolution of the electronics used for the measurement. In estimating the importance of each correction one should keep in mind that for a typical drift velocity of 5 cm/µs a timing error of 1 ns corresponds to a space error of 50 µm. The timing fluctuations introduced through the longitudinal diffusion of

the drifting electrons and the statistical fluctuation of cluster formation along a track are the basic limitations in any chamber resolution. The cluster fluctuations dominate near to the wire (d < 5 mm). The resolution due to diffusion is of the form

$$\sigma_d^2 = A^2 + B \cdot d.$$

This term dominates for d > 1 cm. It has been shown [16] that σ_d can be effectively reduced by going to higher pressure, with $\sigma_d \propto 1/\sqrt{p}$. This is one reason why the JADE detector is operated at 4 atm.

A second timing fluctuation comes from a high frequency noise superimposed onto the leading edge of the chamber signal. For a given discriminator setting and a given chamber signal this noise leads to $\delta t \sim 0.7$ ns [17] in a typical charge division configuration.

A third fluctuation is caused by the slewing characteristics of the discriminator and depends on pulseheight, risetime and threshold setting. In the case of detectors which use charge division readout and therefore record the signal charge this fluctuation can be corrected.

To obtain the true drifttime a number of timing corrections have to be applied to the observed timings : The individual time off-set of all wires must be eliminated and the overall timing has to be adjusted with respect to a common T_0 (in case of e^+e^- storage rings this T_0 is given by the beam crossing). For detectors of large dimensions the time of flight of particles from the innermost to the outermost wire must be taken into account (typically 3 nsec) as well as the signal propagation time along the sense wires (4-5 nsec/m).

The resolution of the time measurement itself differs from experiment to experiment and is dependent on the electronic systems used which will be discussed in more detail later. The resolution values, (σ), as quoted by the different experiments are : MARK II 0.3 nsec for the TAC, TASSO 0.75 nsec (TDC), CELLO 0.92 (TDC), UA1, AFS 1.15 nsec (TDC), JADE 2.17 nsec (TDC). The MARK II experiment quotes also a number for the time resolution obtained for the full system which is 0.9 nsec to be compared with the TAC resolution alone of 0.3 nsec.

3.3 Time-to-space relation

If a drift chamber is operated in a magnetic field orthogonal to the electric field the electrons drift in direction of the Lorentz force. The drift trajectories are therefore rotated by the Lorentz angle α_L

$$\tan \alpha_L = k(E) \cdot V_D \frac{B}{E}$$

with respect to the trajectories for B = 0. The factor k depends on the chamber gas and the electric field. For an ideal driftchamber the time-to-space relation is given by equation (7)

$$d = V_D \cdot t$$

where V_D, the drift velocity, is constant in the entire chamber. In chambers with small driftcells the deviation from the ideal case is biggest. The electric field varies considerably over the region of the cell and therefore V_D changes. One tries to keep this effect small by selecting either V_D or E such that V_D depends only weakly on E. Furthermore, the electrons drift along complicated non linear trajectories (Fig. 12). The length of the shortest trajectory depends on the drift time and on the track angle. The problem to transform the drift time into a distance of closest approach (DCA) is solved by putting the variation of length into an "effective" drift velocity $\bar{V}_D$. In the case of the MARK II detector $\bar{V}_D$ is written as a polynomial in the drift time t which also depends on the track angle α. The driftcell is divided into 3 regions, one close to the sense wire, one close to the potential wires and one in between each region having its own polynomial. The coefficients of the polynomials are determined from real data by comparing calculated space points with the best line fit and minimizing the residuals by varying the coefficients.

Fig. 13a shows the resulting effective drift velocity as function of measured drift time for various incident angles. Fig. 13b shows the effective drift distance as function of the measured drift time. The rather large deviations from a linear correlation are one source of the systematic error in the determination of space points.

For detectors with large drift cells and field shaping electrodes equation (7) can be applied in large areas of each drift cell. This can be seen in Fig. 14 where the electron trajectories and lines of equal drift time are plotted in the vicinity of the wire plane for the case of the JADE detector. This plot is the result of a computer simulation of the electrostatic configuration of one detector cell combined with the measured dependence of the drift velocity and Lorentz angle on the electric and magnetic fields. For a distance of more than 5 mm from the sense wire the electron trajectories are linear. The value of the electric field E in the detector is furthermore chosen such, that V_D is only weakly dependent on E.

In order to transform the measured drift time into a distance d from the anode wire, where d is measured along the center line of each drift space, a timing correction ΔT has to be applied. It is derived from the calculated drift trajectories and describes the time difference between the first electron arriving at the wire and the electrons coming from the center line of the drift space. ΔT depends on the drift time t and the angle of the track with respect to the wire plane. The time-to-space relation then has the form

$$d = V_D (t + \Delta T) \quad .$$

If a track crosses several electrically separate cells, care must be taken to properly match the electric fields (and thereby the drift velocities) in the different regions. An error of 0.2% in V_D leads to a systematic shift of the space points by 100 μm for a track passing 5 cm from the wire plane.

The results obtained by the different experiments for the space resolution in the Rφ plane are summarized in Table 1. This table shows also the dominant limitations in the detectors. MARK II, TASSO and CELLO are mainly limited by mechanical inaccuracies and uncertainties in the time-to-space relation. This can be seen in Fig. 15 which shows $\sigma_{R\phi}$ for the TASSO detector as function of the distances x from the sense wire, for different angles of inclination. For x > 10 mm, where tracks are closer to the potential wires than to the sense wires, $\sigma_{R\phi}$ deteriorates rapidly. It is interesting to note, that the resolution obtained in the CELLO chamber operating at 13 KG is similar to that of TASSO and MARK II both of which operate in a field of 5 KG.

The resolution obtained in the AFS chamber is at present limited by the matching of drift-velocities in the different cells. Furthermore a systematic layer-to-layer variation of the resolution is observed which is probably caused by the wire staggering.

Fig. 16 shows the resolution $\sigma_{R\phi}$ in the JADE chamber as function of the drift time. A contribution of 110 μ to the resolution is due to the TDC, to be added in quadrature to a gas specific contribution of 55 μ. In addition a clear dependence of the resolution on the drift length due to diffusion can be observed. The resulting mean resolution per cell is 155 μ for the small cells and 165 μ for the large drift cells. The mean resolution for a full track through 3 cells is 180 μ. This deterioration is attributed to an imperfect matching of the different drift velocities.

In conclusion one can say that the main limitations of the resolution in the Rφ-plane are systematic errors such as mechanical alignment, electronic resolution and knowledge of the time-to-space relation. Deterioration of the resolution due to diffusion can be seen in the case of large drift distances but the diffusion is not a limiting effect at present. What is needed to improve the resolution is: good mechanics and good surveying, fast electronics, gases with little diffusion and a chamber design which permits the use of a simple time-to-space relation.

4. MEASUREMENT OF THE z-COORDINATE, z RESOLUTION

There are five methods in use for the determination of the third coordinate which is in most cases the coordinate along the axis of the cylindrical chamber.

i) small angle stereo : This method is used in most of the classical drift dhambers. The z coordinate is directly related with $\sigma_{R\phi}$.

$$\sigma_{RZ} = \sigma_{R\phi} \; / \sin \alpha_s$$

where α_s is the stereo angle. Typically one has $\sigma_{RZ} = 20 \cdot \sigma_{R\phi}$ leading to a resolution $\sigma_{RZ} \sim$ 4-5 mm. The disadvantages are that the stereo planes

cannot be used for pattern recognition and that in the case of high density jets ambiguities can occur in the correlation of the Rφ- and z-coordinates.

ii) delay line readout : Here delay lines run parallel to the anode wires. The induced signal from an avalanche at the anode wire is measured at both ends of the delay lines. This method is used in the driftchambers of the CCOR-experiment.[3] A resolution of $\sigma_{RZ} \sim 5$ mm is obtained for delay lines with a length of 80 cm - 150 cm. One problem is that delay lines add a considerable amount of material to the chamber.

iii) cathode strip readout : This readout method is used in the chambers of PLUTO, DESY-Heidelberg and CELLO. The proportional chambers of CELLO have cathode strips under 90^0 and 30^0 with respect to the sense wires. The correlation between both strips is done through a measurement of the pulseheight. A resolution of $\sigma_{RZ} = 0.4$ mm has been reached for tracks at $\theta = 90^0$. Fig. 17 shows the z-resolution as function of θ.

In all three methods mentioned so far the z-coordinate can only be measured independently of the Rφ-coordinate. In pictorial drift-chamber systems where one measures space points two other methods are used.

iv) charge division : This method is used in JADE, the AFS and UA1 experiments. The integrated charge from each hit is measured at both ends of the signal wire. The ratio of the charges determines z and the sum of both charges measures the energy loss dE/dx of the particle in the chamber gas. Since the two amplitudes are recorded together with the signal timing, true space points are measured. The resolution $\Delta l/l$ of the charge division is limited by the signal to noise ratio [18]. The resolutions which have presently been obtained by applying charge division are $\sigma_z = 1.6$ cm ($\Delta l/l = 0.6\%$) in JADE (Fig. 18) and $\sigma_z = 1.7$ cm ($\Delta l/l = 1.2\%$) in AFS. Problems in this technique arise if two tracks are so close to each other that the signal charges overlap within the integration time. In this case the z-information cannot be used.

v) drifttime measurement : This method will be used by the TPC. In this detector the electrons drift parallel to the beam axis towards the endplates of the chamber. Their arrival time with respect to the time of the bunch crossing measures directly the time of drift and therefore the z-coordinate.

5. CHAMBER ELECTRONICS

In most of the classical driftchambers only the drifttime is recorded either in Time to Digital Converters or Time to Analog Converters. Both systems have advantages and disadvantages. A detailed comparison can be found in an ECFA-LEP report [19]. In most cases the electronics will accept only a single hit per wire. In pictorial driftchambers one measures the drift time and the signal charge with a multihit electronics in order to achieve good double track resolution. This is done in several ways which will be shortly discussed : The AFS has in its TDC system (the CERN-DTR system) a multihit electronics whereas signal amplitudes are measured only for the first hit on each wire. The information on dE/dx and z is therefore lost for all subsequent hits. The JADE jetchamber has a genuine multihit electronics (for 8 hits/wire) which is described in detail elsewhere [20]. This electronic system has been in operation for over one year and shows excellent longterm stability (1-2%).

Two techniques with possibly great potential are being investigated by the TPC and UA1 groups. In the case of the TPC the shaped response signal for each wire and pad is fed into an analogue storage device (CCD), which is capable of storing both pluseheight and time information. This analogue shift register samples the input waveform at a rate determined by an external clock. The resultant levels are shifted along until the entire history of an event is completely stored, a time interval corresponding to the maximum drift time. The CCD's permit the TPC to be subdivided electronically into several million independent sensitive volumes. Only in the case of a good event trigger will the contents of the CCD's be read out and digitized.

The second approach, used in the UA1 central detector [21], is based on fast analog-to-digital converters (FADC). These flash ADC's consist of 63 strobed differential comparators (for a 6 bit ADC), a resistor string to provide the reference voltages and a 63 to 6 encoder. One of the inputs of each comparator is connected in parallel to the signal input, the other to a reference voltage. In the UA1 application 2 FADC's per wire are used, the first gives directly the track's position along the wire by the charge division method. The second FADC has a "logarithmic" response and is used for the measurement of the energy loss dE/dx. The FADC's used in this experiment have a sample time of 32 nsec, necessitating the integration of the signal charge over a period of 32 nsec.

The great amount of information per event provided by each of these two methods is very welcome in the analysis but will require special attention in the data handling.

6. DOUBLE TRACK RESOLUTION

The high local density of tracks as it occurs for example in the hadronic final states in e^+e^- annihilation requires a good double track resolution. The limiting factors depend mainly on the electronics. In driftchambers with single hit readout the minimal separation between tracks is given by the wire spacing.

In the case of the JADE detector with its multihit electronics the separation is given by the integration time which is chosen. Since this time is adapted to the signal form of the chamber pulse one could say that the double track resolution is determined by the pulseform.

For all detectors except TPC the double track resolution Δd means that tracks within a volume V = (Δd * chamber radius * chamber length) cannot be resolved, since tracks with the same coordinates in $R\phi$ but with different z cannot be distinguished. In the case of the TPC this volume is much smaller since it is defined by the double track resolution in the $R\phi$ plane (Δd) and in z direction (Δz) : V = (Δd * Δz* chamber radius).

Typical values for the resolution are : Δd = 1.6 cm (TASSO), Δd = 0.7 cm (JADE) and Δd = 2.4 cm, Δz = 2.1 cm (TPC).

The loss of entire tracks due to the finite double track resolution depends strongly on the topological and kinematical configuration of the observed events. An analysis of the multihadron events at E_{cm} = 30 GeV seen in the JADE detector shows that 0.2% of all tracks in jets are lost.

7. COMMENT ON dE/dx

The question of particle identification through the measurement of dE/dx is discussed in detail in two other reviews at this conference [22,23]. In this chapter only a few comments are made which concern detectors combining particle tracking and identification.

The method of multiple sampling of the energy loss in the gas is used. This is an elegant and powerful solution since it allows particle identification with the same high granularity which is desired for track direction measurement. Certain compromises and corrections have to be accepted in order to reach reasonable resolutions for tracking and identification of particles : The large angular acceptance in θ (for full solid angle coverage) creates large variations in the amplitude corrections, mainly due to angle dependend saturation effects. The use of charge division requires a gas gain which is larger than one would like for particle identification. One has to make a compromise between charge collection time and double track resolution. (This is somewhat dependend on the electronics system). The use of gas at elevated pressure helps in reaching a good space resolution also for long drift length and increases the resolution for particle identification for a

given detector diameter. On the other hand the momentum region in which particles can be separated by 3σ for example decreases since the Fermi-plateau starts at lower momenta for higher pressure. Furthermore it is at present not clear if the improvement in resolution is proportional $1/\sqrt{p}$ [24].

One important factor entering the effective dE/dx resolution of a chamber is the tracklength usable for energy loss sampling. It is on the average shorter than the longest possible track length due to partial overlap of tracks. The amount of overlap depends strongly on the event configuration. In Fig. 19a the distribution of hits/track in JADE is shown for tracks in the momentum interval 1-2 GeV/c from e^+e^- annihilation at 30 GeV. Fig. 19b shows the mean number of hits/track and the width of the hit distribution as function of track momentum. On the average the track length is 30 cm compared with a possible length of 48 cm. This problem is inherent to the event structure and cannot be avoided. One consequence is to go to detectors with greater radii.

8. CALIBRATION

It can be said without too much exaggeration that the space resolution and particle identification are to a large extent determined by the quality of the calibration of the system. Two main points concerning calibration have been discussed in other reviews at this conference : Electronic calibration [25], and the use of lasers and X-ray flashtubes for calibration [7]. Laser ionization of the chamber gas along a well surveyed line may provide a powerful tool for the mechanical calibration of large driftchambers and the determination of drift velocities as well as effects of the magnetic field.

The wire dependend calibration of the gas gain will probably need real data which are rare at PETRA and are hopefully plenty on top of the Z^0 at LEP. Cosmic ray events help at PETRA and are rare 1000 m below the Jura.

9. EXTRAPOLATION TO LEP

Summarizing our present experience with large driftchamber systems one can say that classical driftchambers work reliably in many experiments and that the ambitious concept of pictorial drift chambers has been made to work in large scale applications. The jet chamber of the JADE detector which is the first large imaging driftchamber used in an experiment has been operating now for over one year and the design goals have been well met. Based on present experience with this type of chamber one can hope to obtain a space resolution in the $R\phi$ plane of the order of 100 - 120 μ through fast electronics, laser calibration of the wire position and the drift velocity and the choice of a chamber gas with smaller diffusion than Argon-Methane (e.g. Propane). It does not seem realistic to hope for resolutions much better than 100 μ in large chamber systems.

For a central detector of a LEP experiment one could imagine three scenarios all of which would use pictorial driftchambers. This clearly is a very personal choice and the order of presentation follows a line of increasing scepticism. The reason for the choice of pictorial driftchambers is the combination of good space resolution, good track finding and pattern recognition and particle identification.

A first secnario would be a central detector à la JADE. The detailed realization depends on several parameters. Earlier discussions on LEP detectors were based on solenoids with fields of 10 - 15 KG. This high field solution helps to keep the detector smaller (chamber radius and length are smaller than in the low field solution at the same performance). One has however to increase the driftfield in the chamber to several kV/cm in order to keep the Lorentz angle α_L below 20^0 (which is advisable). This can create technical problems. More important however is the problem of tracks overlapping with each other which leads to a loss in effective tracklength usable for dE/dx. Since tracks from a common origin fan out with increasing distance from the vertex a chamber with large radius would be of clear advantage. The magnetic field would be lower for a large radius chamber and the Lorentz angle α_L consequently smaller. Problems with this solution are cost and the increase in wire length if one wants to cover the same solid angle. Rough estimates lead to wire lengths in

excess of 6m which creates problems for charge division accuracy and wire position due to sagging.

Even the large radius solution however is not large enough to operate the chamber at atmospheric pressure if one wants to achieve a reasonable particle identification through ionization sampling. The most suitable value for the pressure depends on the chamber gas, radius, effective track length and maximum momentum at which one would like to identify particles.

A few constructional details could be different in comparison with JADE: The wire planes of the sectors should not point at the origin but should be tilted by a few degrees. This avoids singularities in the resolution for high momentum tracks running over their full length close to the wire plane. Furthermore this arrangement could compensate a few degrees of the Lorentz angle. In addition one would try to have fewer radial segmentations in order to obtain better track matching and resolution.

The flash ADC's mentioned already in context with the electronics of the UA1 experiment have rapidly developed over the last years thanks to the boom in video technique. One can now obtain FADC's with a sample time of 10 ns [26]. Two fast FADC's of this kind together with two RAM's per wire would constitute a very powerful read out electronics : One could measure the center of gravity of the drifting electrons to $\sim$ 1 ns and hopefully reduce the deterioration in resolution due to diffusion. One could obtain a double track resolution of $\sim$ 2.5 mm (Δt = 40-50 ns) and improve the dE/dx resolution through sampling of the baseline (which can be shifted due to old ions in the drift region) before the signal.

A second scenario would use a Time Projection Chamber as central detector. This possibility is discussed elsewhere [14].

The third scenario differs from the frist two insofar as it tries to incorporate "cluster counting" [23] as method of particle identification. Since cluster counting aims at a higher resolution than ionization sampling it permits a better particle separation. On the other hand one cannot do cluster counting and high accuracy coordinate measurement with the same detector element. A central detector with cluster counting would therefore have to combine high resolution drift-chambers with chambers for cluster

counting. The optimal resolution using N drift chambers is obtained by an arrangement of three groups [8] : N/4 chambers each at R_{min} and R_{max} and N/2 chambers in the center of the detector. Between these three rings one could do the cluster counting. The feasibility of such a detector and its layout depend entirely on the progress made in cluster counting.

According to the present schedule there is less than one year left before the first proposals for LEP detectors will be submitted. This time should be used to improve the understanding of the existing detectors and in particular the dE/dx measurement. The use of Lasers for chamber calibration has to be studied in detail and experience has to be gained with FADC's. But all things considered hopes for powerful central detectors at LEP are high.

ACKNOWLEDGEMENT

I would like to thank Dr. R.D. Heuer for his help in preparing this report and the members of the various detector groups for their information and helpful discussions. I am very grateful to the organizers of the Uppsala Conference for their warm scandinavian hospitality.

TABLE 1

Resolution in the Rφ plane and its limitations

Detector	Average $\sigma(R\phi)$	Limitations
MARK II	$\sim$ 210 μ	mechanics, time-space relation
TASSO	$\geq$ 220 μ	mechanics, time-space relation
CELLO	210 μ	TDC resolution, mechanics, time-space relation
AFS	250 μ	matching between cells, layer-to-layer variation
JADE	180 μ	TDC resolution $\approx$ 110μ, diffusion, cell matching

FIGURE CAPTIONS

Fig. 1 : a) Schematic drawing of the TASSO drift chamber (dimensions in mm)
b) Drift cell geometry of the TASSO chamber

Fig. 2 : A hadronic event at 30 GeV c.m. energy as seen by the TASSO chamber. Only the hits in the 0^0 layers are shown.

Fig. 3 : Schematic view of the central tracking detector of CELLO

Fig. 4 : A hadronic event at 35 GeV c.m. energy as seen by the CELLO chamber.

Fig. 5 : Cross section through two segments of the jet-chamber of JADE. d is the length of the drift path, α the Lorentz angle.

Fig. 6 : A hadronic event at 35 GeV c.m. energy as seen by the jet chamber of JADE. Hits assigned to tracks by pattern recognition are shown as crosses, unassigned hits as dashes.

Fig. 7 : Layout of the AFS drift chambers

Fig. 8 : High p_t event as seen by the AFS driftchamber at the ISR. Shown are all points used in the track fitting.

Fig. 9 : Orientation and structure of the wires in the central and forward chambers of the UA1 experiment.

Fig. 10: Schematic drawing of the Time Projection Chamber

Fig. 11: Graphical summary of important dimensions of several large drift-chamber systems. Left picture : Radial position and number of sense wires along a track. Right picture : Maximal driftlength.

Fig. 12: Schematic drawing of different drift paths within a cell (MARK II)

Fig. 13 : a) Effective drift velocity vs. measured drift time at various incidence angles, for small and large cells
b) Effective drift distance vs. measured drift time at various incidence angles for small and large cells. The functional form is plotted beyond the physical region of the cell (both plots for MARK II).

Fig. 14 : Drift trajectories and lines of equal drift times (dashed curves) for the JADE configuration. (α = Lorentz angle)

Fig. 15 : Spacial resolution achieved in TASSO chamber, measured with Bhabha events and hadronic events. The resolution for 0^{o} layers is plotted vs. the position in the cell for various entrance angles.

Fig. 16 : Mean rms deviation of single cell track fits in the (R-ϕ)-plane as function of the mean drift distance. The arrows indicate the cell dimensions in ring 1-3 respectively (JADE).

Fig. 17 : z resolution as obtained with the cathode strip readout in the CELLO proportional chambers as function of the polar angle θ.

Fig. 18 : Distribution of rms deviations for single cell track fits in the R-Z plane as obtained with charge division in the JADE chamber.

Fig. 19 : a) Distribution of number of hits per track (with momenta 1-2 GeV/c) with in jets of multihadronic events at 35 GeV c.m. energy as seen in the JADE chamber.
b) Mean number of hits per track and rms of hit distribution as function of momentum.

REFERENCES

1) L. Criegee et al., Proc. of the 1973 International Conference on Instrumentation for High Energy Physics, pg. 707 (1973)

2) A.H. Walenta, IEEE Trans Nucl. Sci. 22, 251 (1975)
W. Bartel et al., Phys.Lett. 64B, 483 (1976)

3) L. Camilleri et al., Nucl.Instr. and Meth. 156, 275 (1978)

4) W. Davies-White et al., Nucl.Instr. and Meth. 160, 227 (1979)
R.H. Schindler, SLAC-219 (1979)

5) Proposal for a PEP facility based on the Time Projection Chamber (TPC), LBL-UCLA-Yale-Riverside-Johns Hopkins, Spokesman : D.R. Nygren, LBL, Proposal PEP4 (1976)

6) Proposal for a Compact Magnetic Detector at PETRA (JADE), DESY-Hamburg-Heidelberg-Lancaster-Manchester-Rutherford-Tokyo, Spokesman : R. Felst, DESY, Proposal PETRA 76/16 (1976);
H. Drumm et al., DESY 80/38 (1980)

7) B. Sadoulet, these proceedings

8) R.L. Gluckstern, Nucl.Instr. and Meth. 24, 381 (1963)

9) H. Boerner et al., DESY 80/27 (1980)

10) W. de Boer et al., MPI-PAE/Exp. El. 84 (1980)

11) J.E. Augustin et al., LAL-80/16 (1980)

12) D. Cockerill et al., 1980 Vienna Wire Chamber Conference, Nucl. Instr. and Meth.,to be published.

13) M. Barranco Luque et al., CERN-EP/80-41

14) D.R. Nygren, these proceedings

15) H. Drumm et al., IEEE Trans.Nucl.Sci. 26.1, 81 (1979)

16) W. Farr et al., Nucl.Instr. and Meth. 154, 175 (1978)

17) Isabelle Summer Study 1978, pg. 147

18) V. Radeka and P. Rehak, IEEE Trans.Nucl.Scie. 25, 46 (1978)

19) Report SSG 11-2, Appendix 1 : L.O. Herzberger - Electronics for MWPC's and driftchambers.

20) W. Farr and J. Heintze, Nucl.Instr. and Meth. 156, 301 (1978)

21) M. Calvetti et al., CERN-EP / 80-42

22) W.W.M. Allison, these proceedings

23) A.H. Walenta, these proceedings

24) I. Lehraus et al., CERN/EF/Beam 80

25) M. Breidenbach, these proceedings

26) Siemens AG : SDA 5010

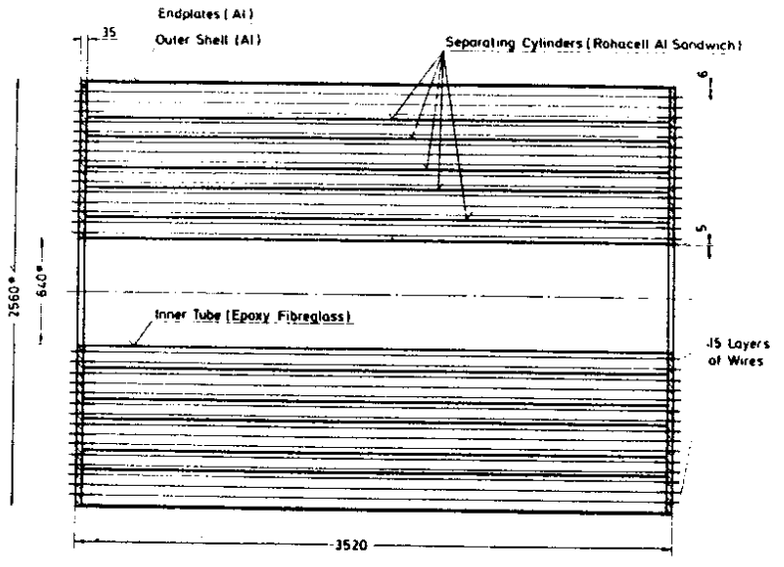

Fig. 1 a)

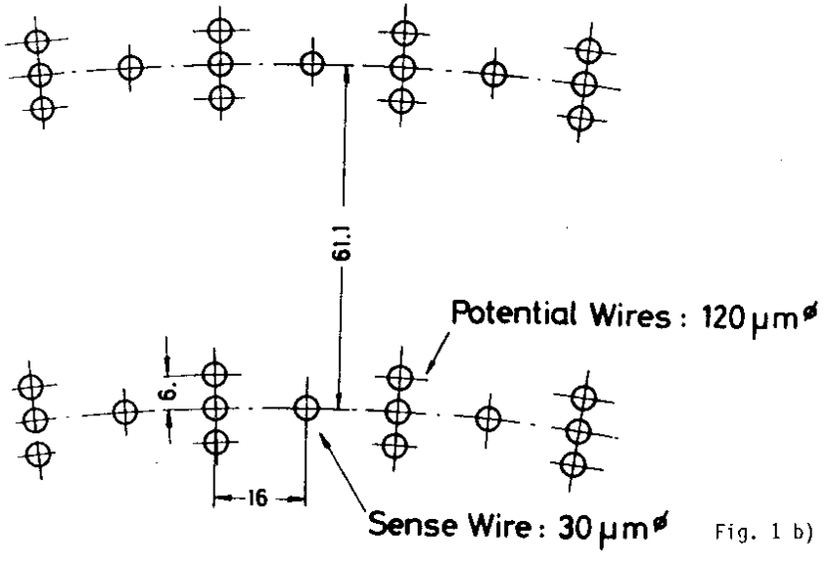

Fig. 1 b)

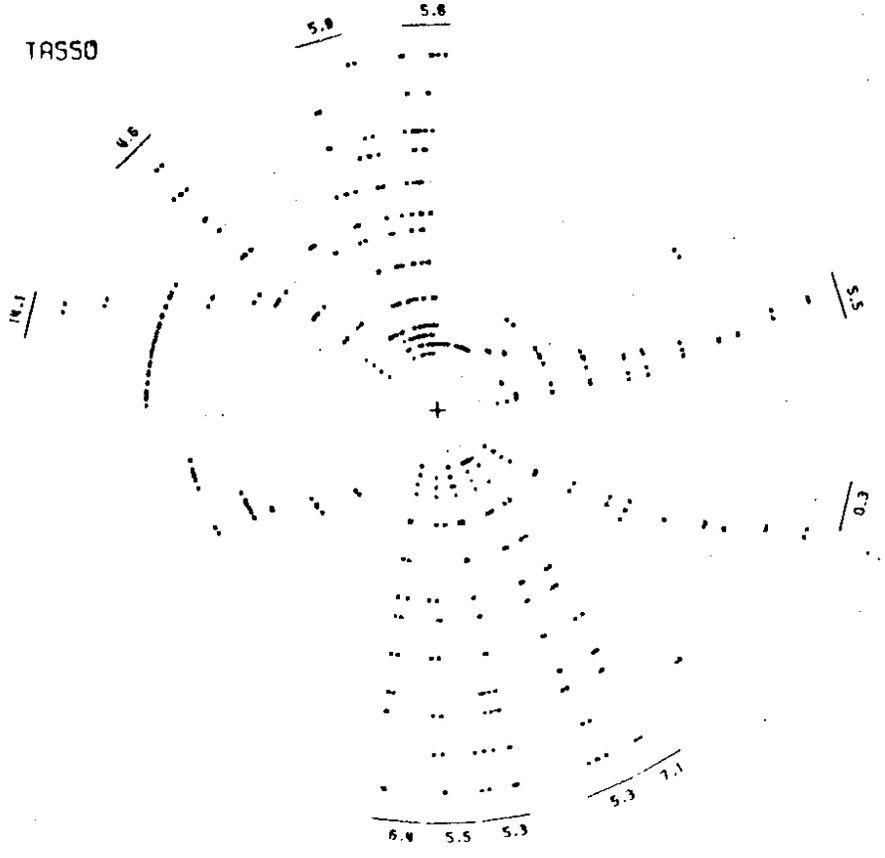

Fig. 2

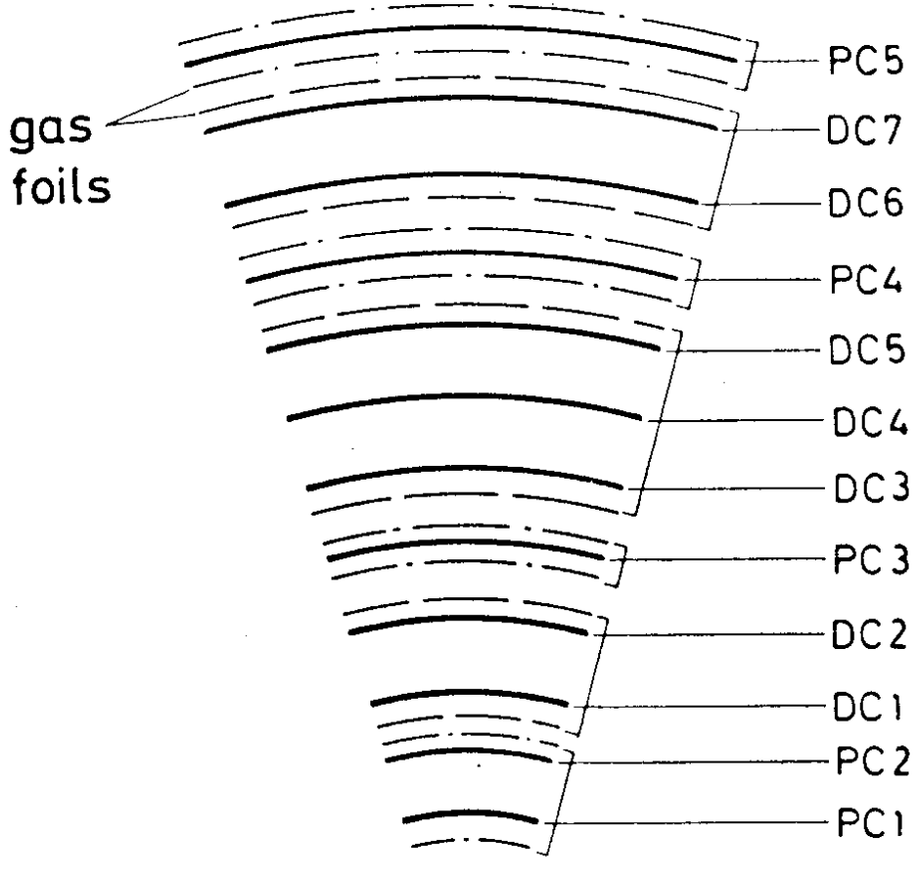

Fig. 3

3G260

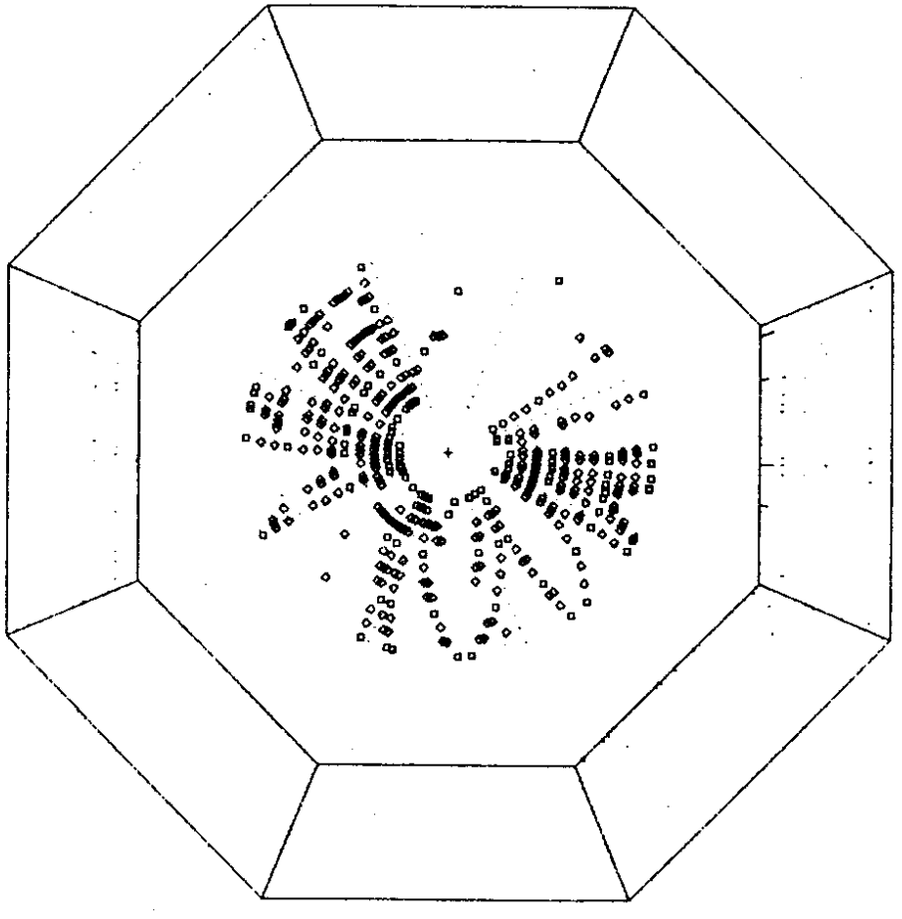

Fig. 4

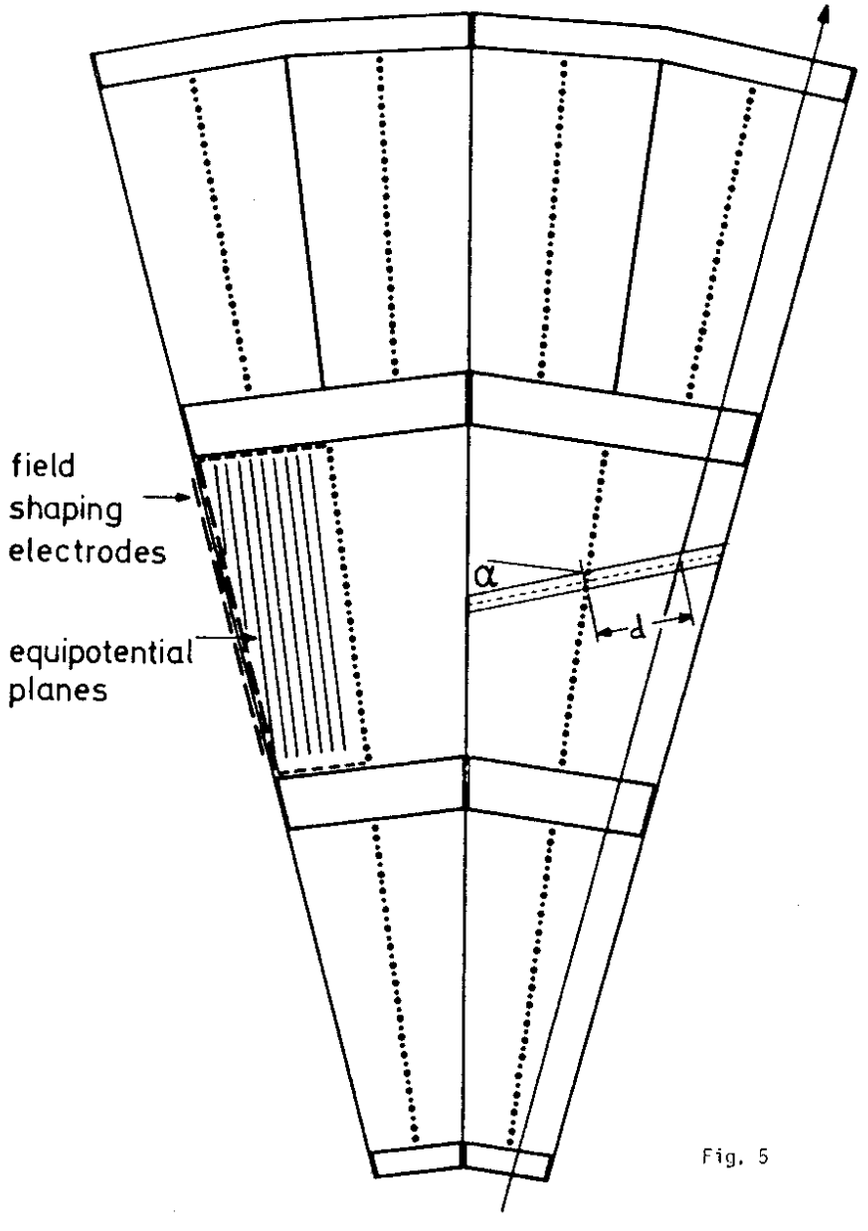

Fig. 5

DSN F22ELS.TPMH435
JADE
R-FI SECTION
BEAM 17.500 GEV
MAG.FIELD -4.534 KG
TRIGGER 0201
DATE 09/06/80
TIME 18.27.20
2892 2226 39
IDHITS 586
ELGTOT 12360
MUHITS 16
LGCYL 12306
LGCAPS 0 54
FWCAPS 0 0
13.2
11.8
9.1
15.4
11.1

Fig. 6

Fonds B
Fonds A
ISR
FOND "B"
FOND "A"

Fig. 7

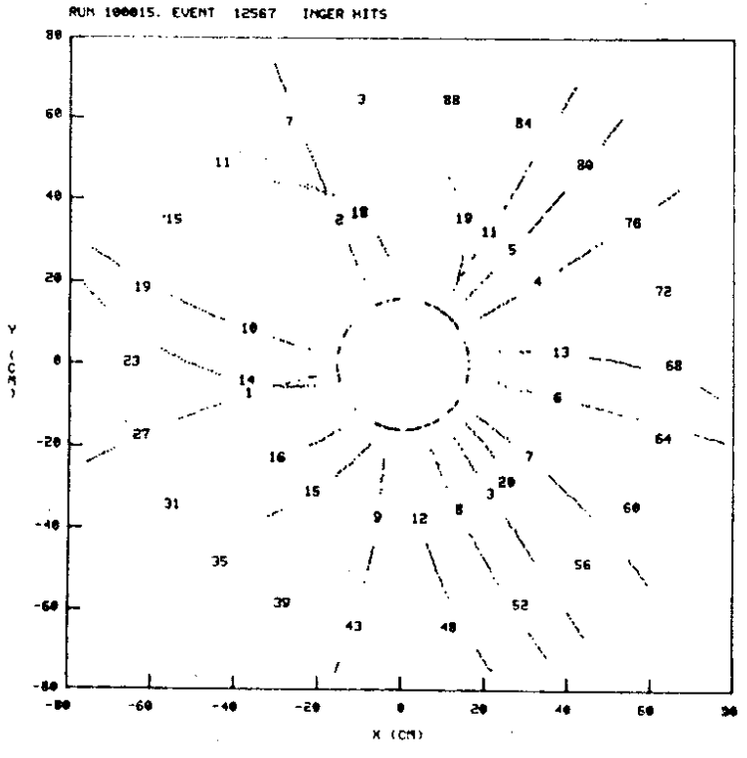

Fig. 8

30266

a) CENTRAL CHAMBER

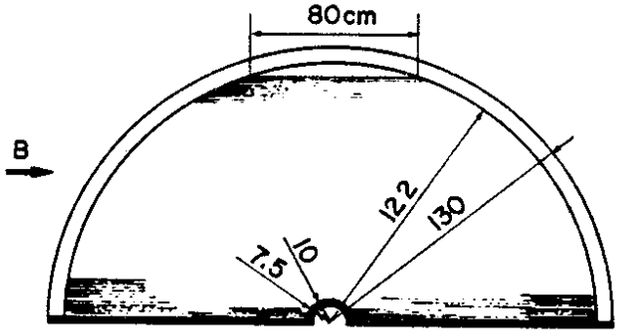

b) FORWARD CHAMBER

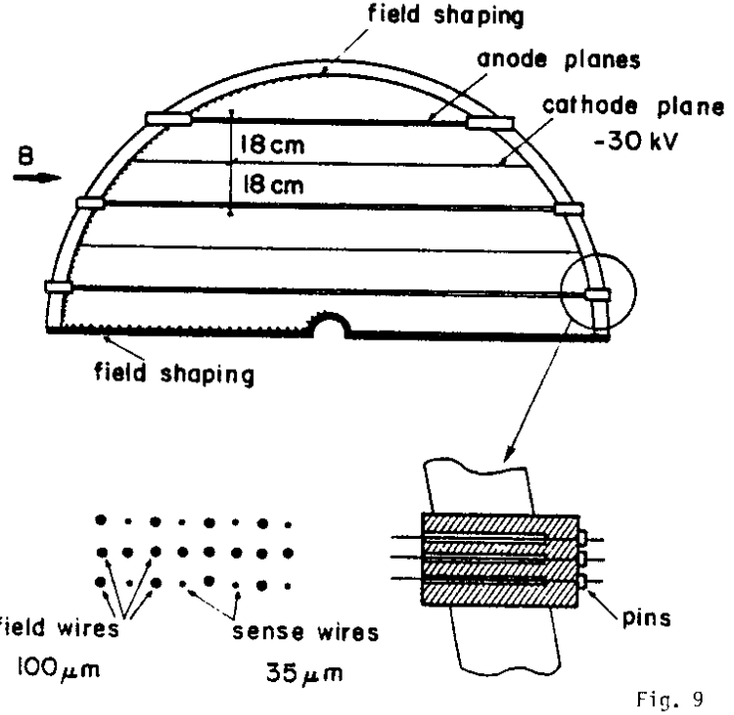

Fig. 9

30261

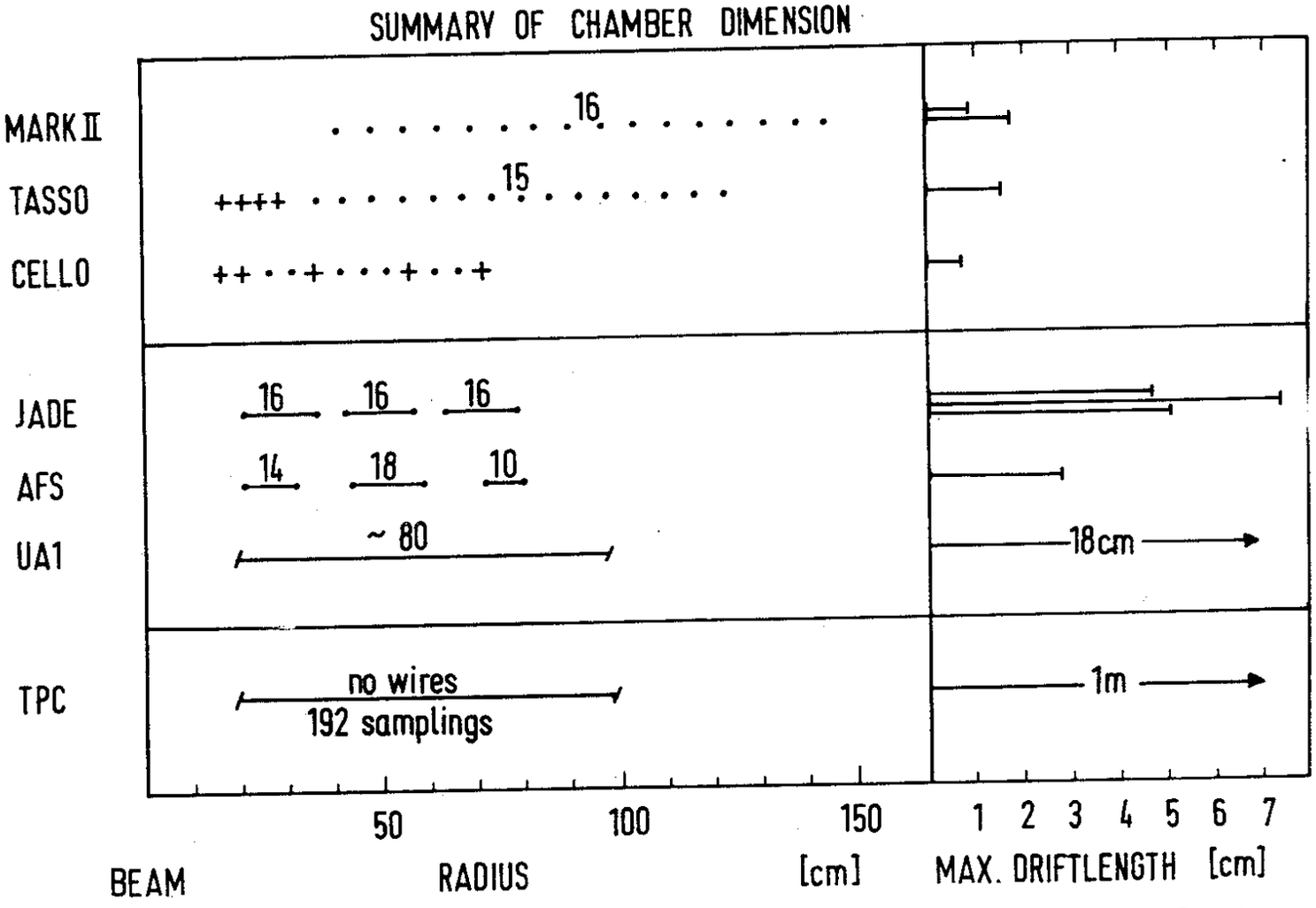

Fig. 11

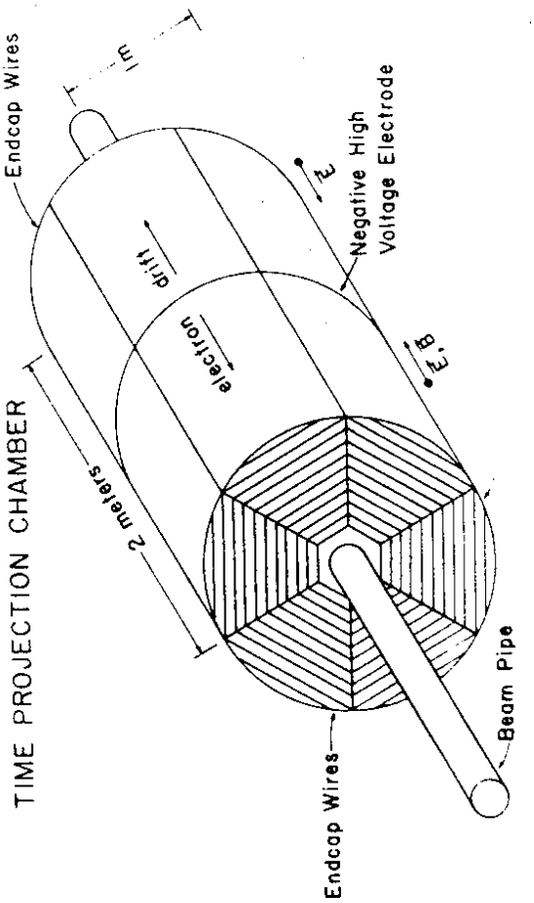

Fig. 10

30267

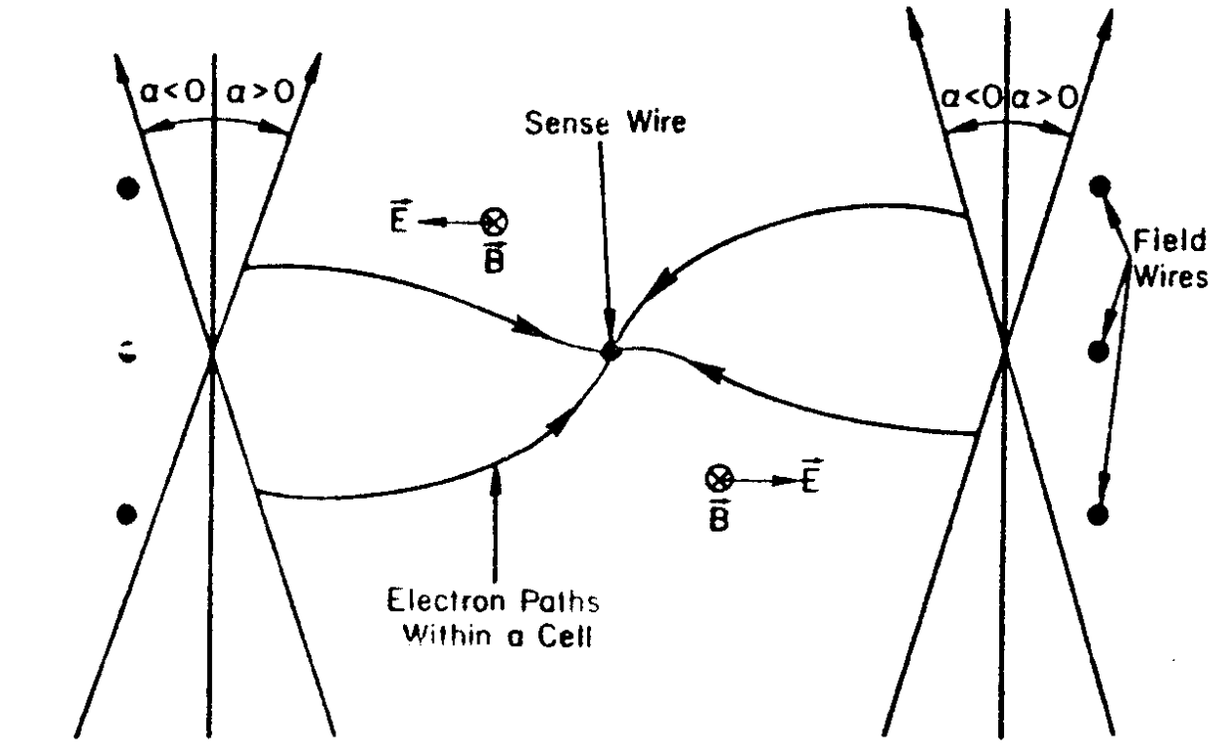

Fig. 12

30270

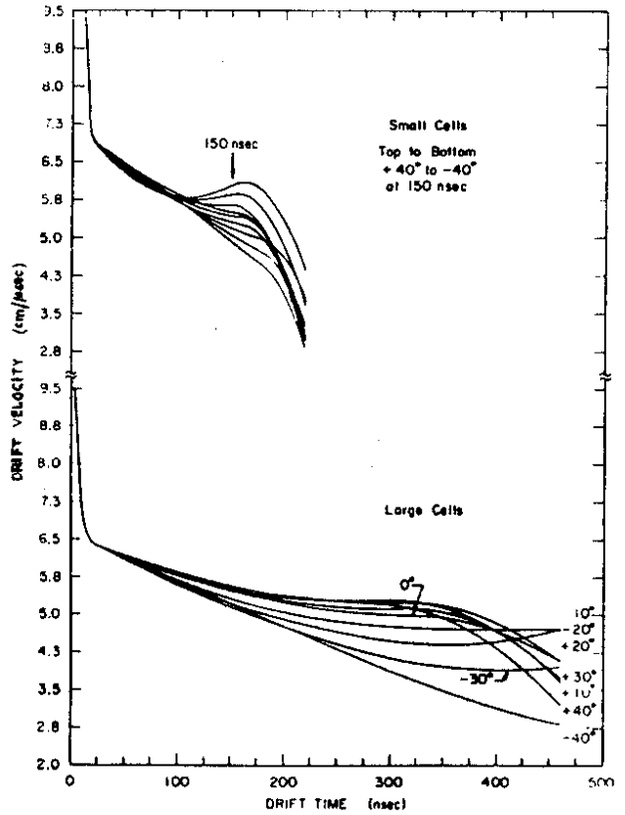

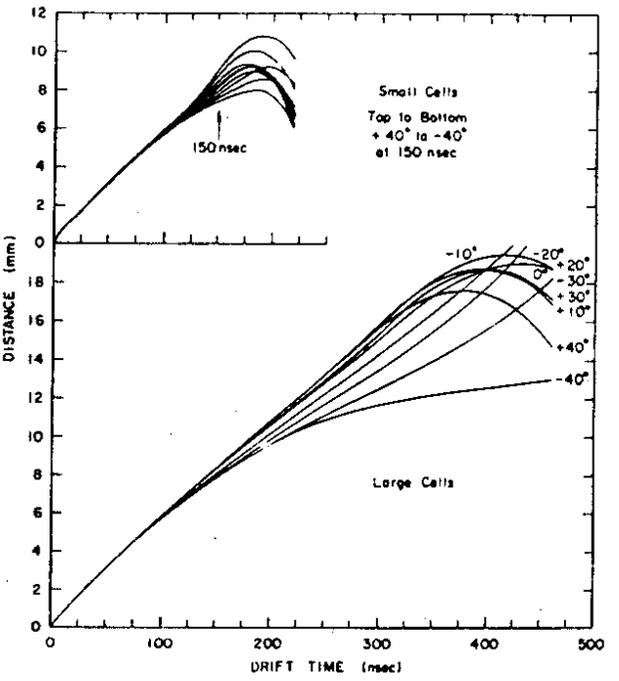

Fig. 13

30274

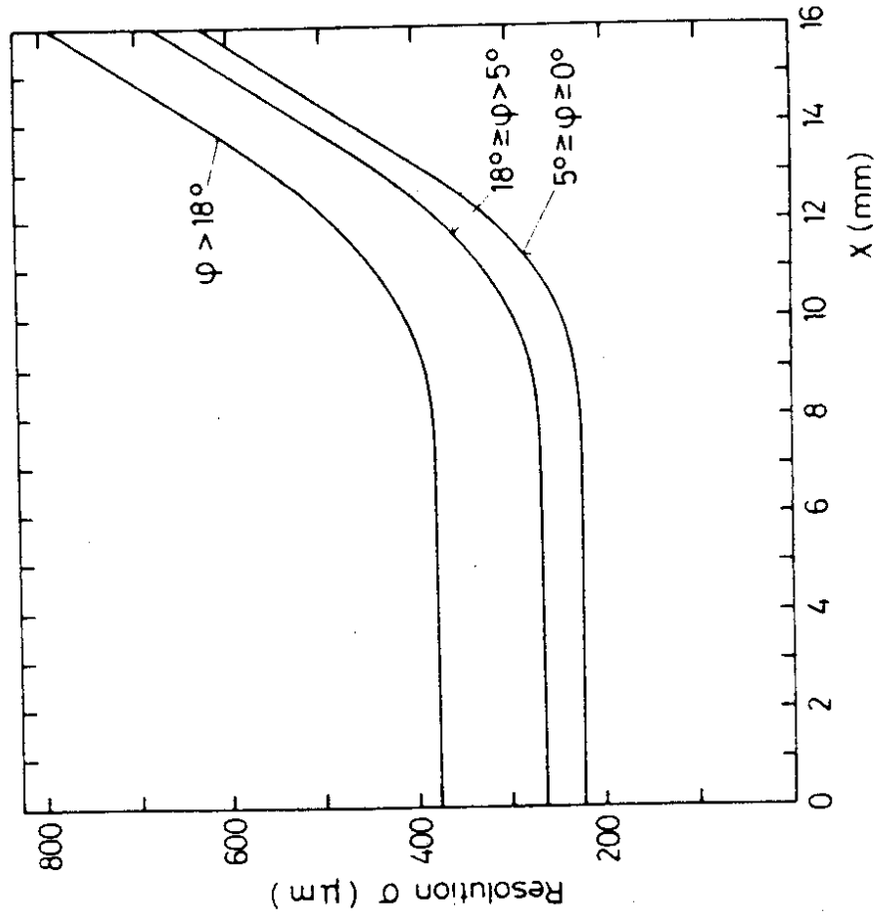

Fig. 15

30265

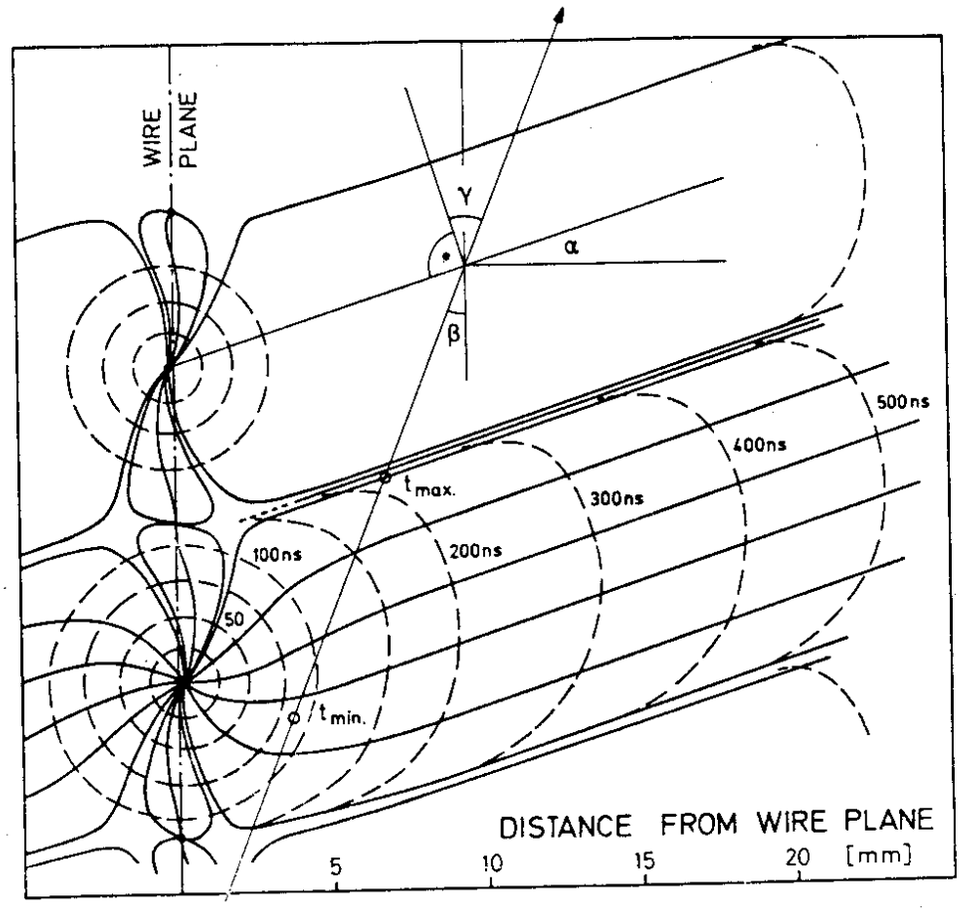

30272

Fig. 14

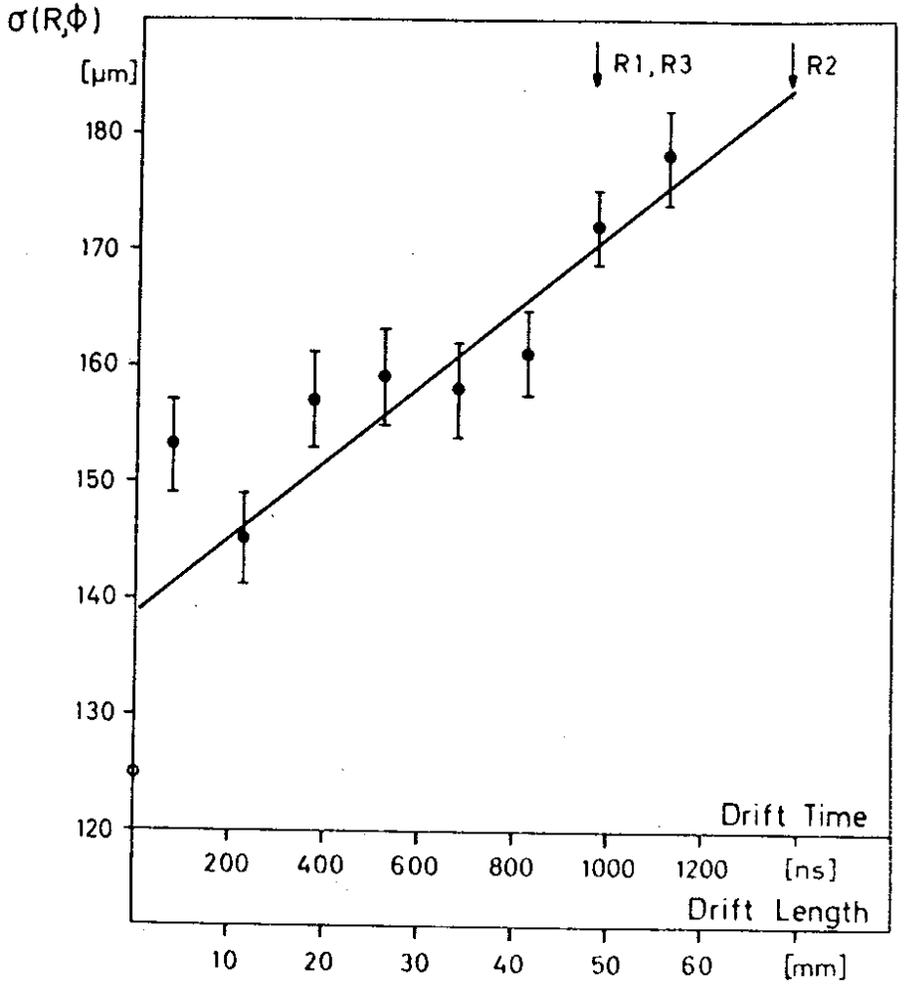

Fig. 16

30255

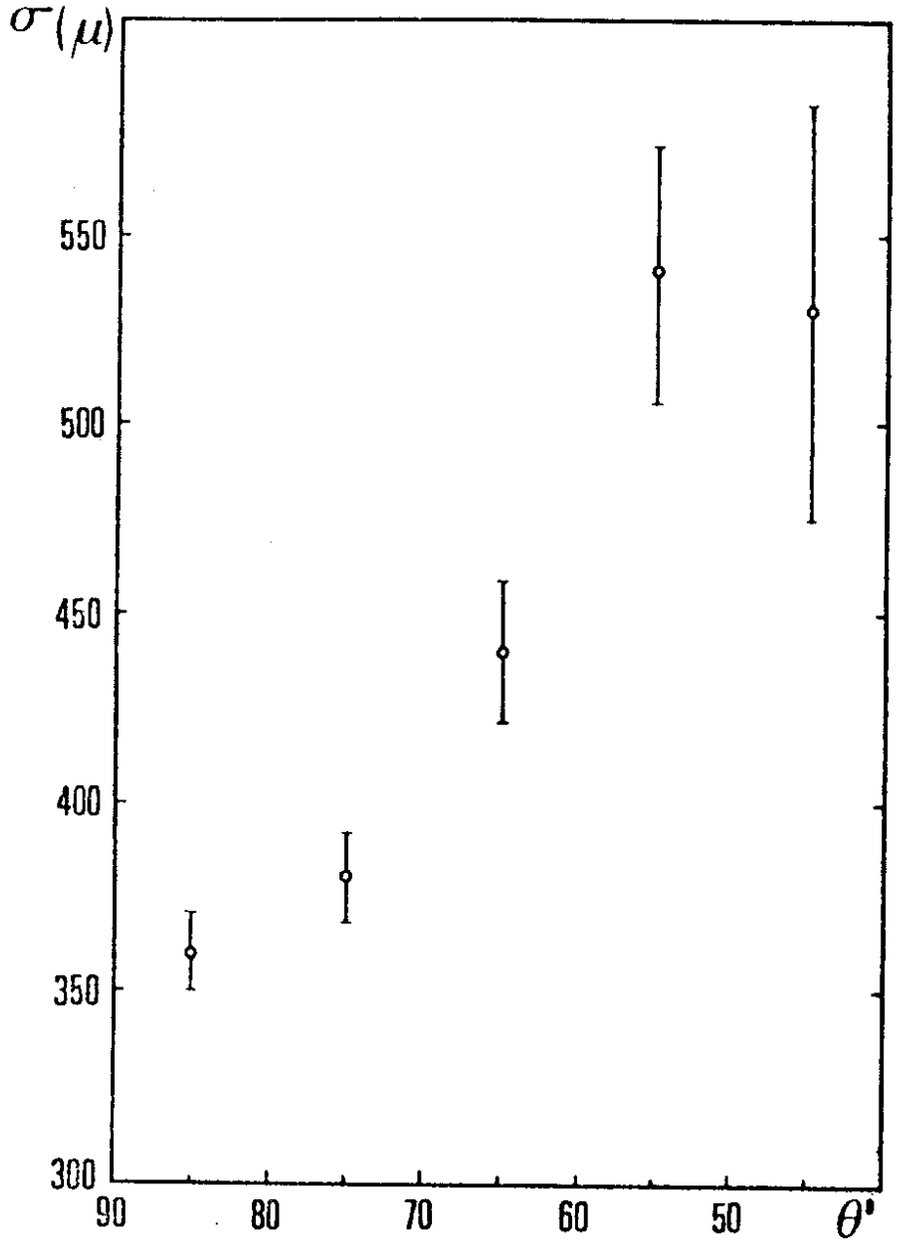

Fig. 17

30257

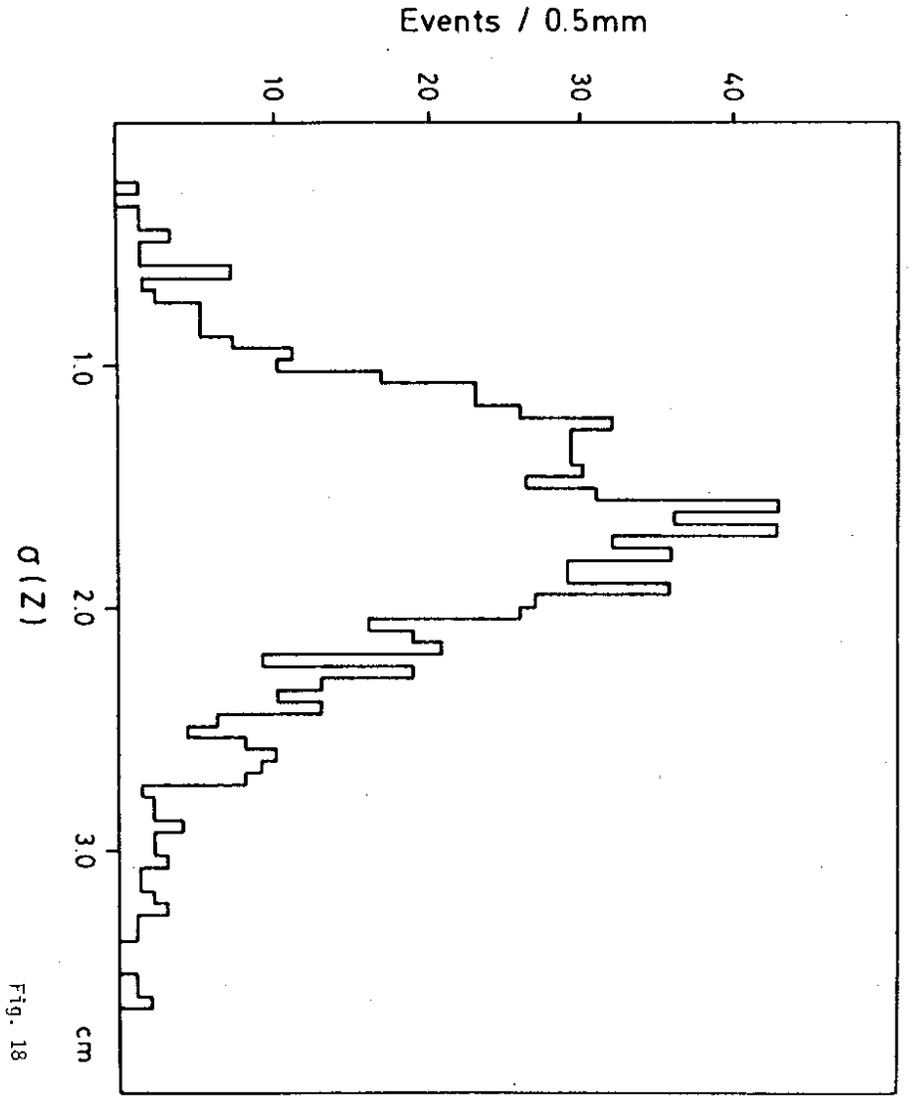

Fig. 18

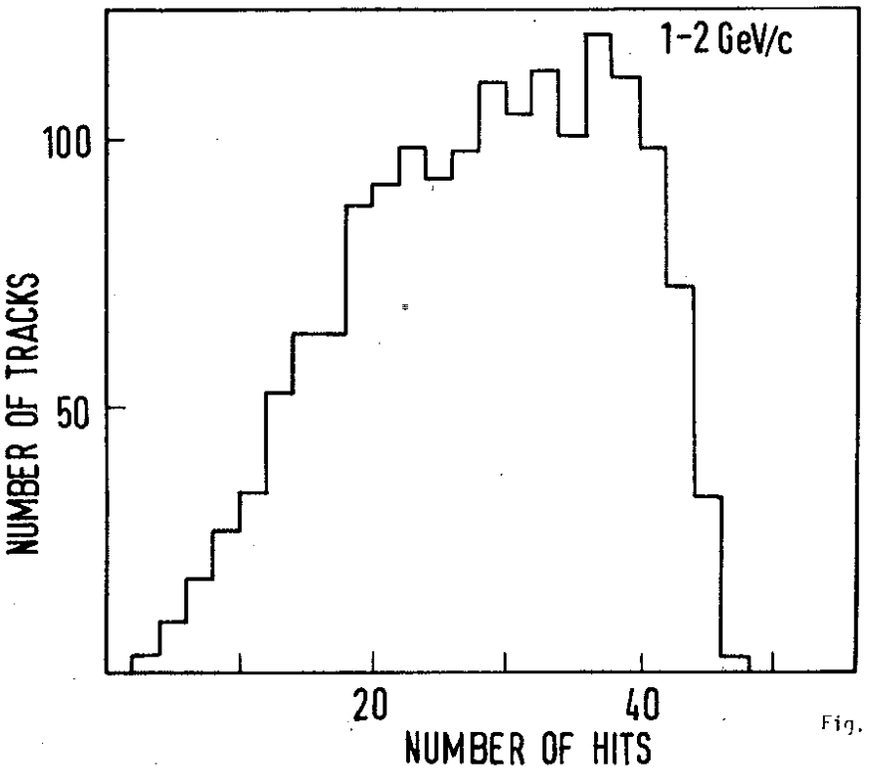

Fig. 19 b)

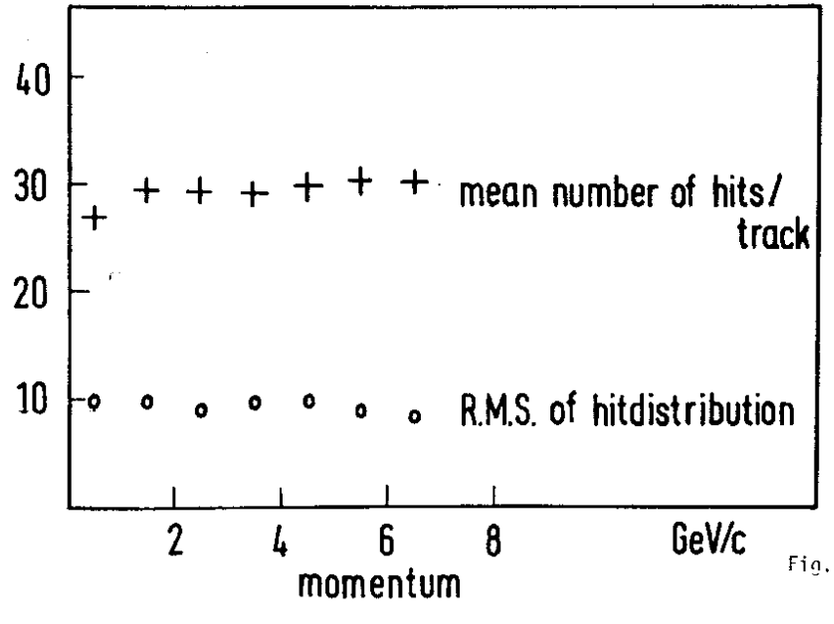

Fig. 19 a)